Chapter 3

Fundamentals

3.1 Image-potential states...

Besides the electronic states derived from the bulk bands and intrinsic surface states such as Tamm [169] or Shockley [159] states, also a peculiar class of states can be found at metal surfaces — image-potential states. The existence of image-potential states at metal surfaces was predicted by Echenique and Pendry [49] in 1978 and a few years later confirmed in inverse photoemission experiments [44, 168]. Excellent and extensive reviews on the physics of image-potential states may be found in e.g. [50, 57, 180, 48].
An electron at a distance z in front of a metal surface is screened by the charge carriers in the metal in such a way that the induced electric field outside of the metal can be described with a positive "image" charge at $-z$, symmetrically below the surface (cf. Fig. 3.1a). The electron is attracted towards the surface by this image charge, i.e. it experiences a Coulomb-like force

$$F(z) = -\frac{e^2}{4\pi\varepsilon_0}\frac{1}{(2z)^2} \ . \tag{3.1}$$

If a gap in the surface-projected band structure prevents the electron from penetrating into the crystal, the electron can be trapped between the crystal and the image potential

$$V(z) = E_{\mathrm{vac}} - \frac{e^2}{4\pi\varepsilon_0}\frac{1}{4z} \ , \tag{3.2}$$

which converges to the vacuum energy E_{vac} with increasing distance from the surface. In this quantum well a Rydberg-like series of bound states forms (schematically indicated in Fig. 3.1b), labelled with the quantum number n

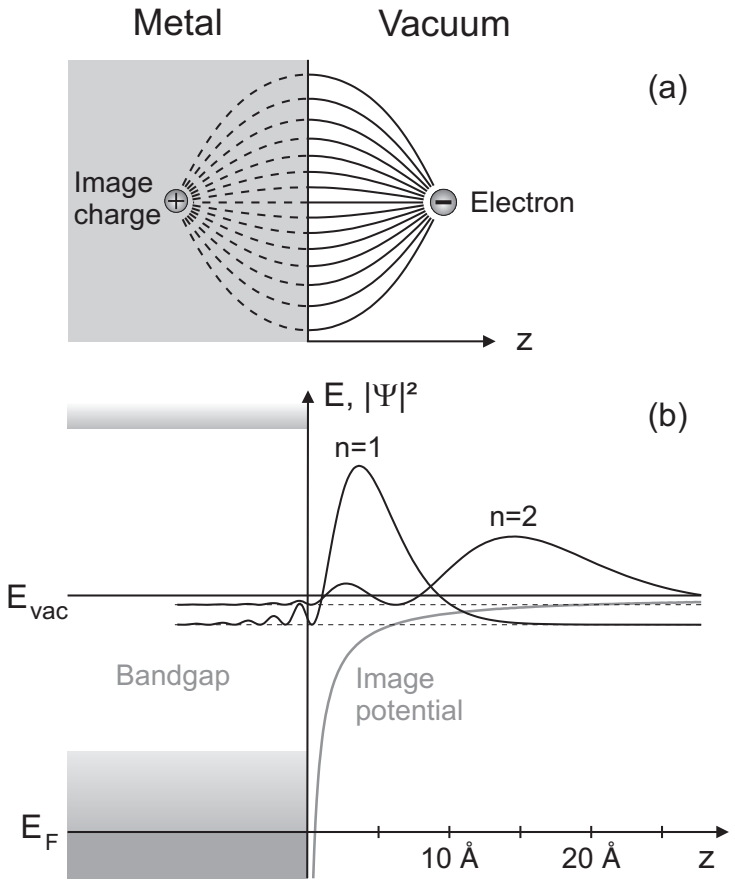

Figure 3.1: The field induced by an electron in front of a metal surface (a); In the quantum well formed by the Coulomb-like image potential and the gap in the surface-projected band structure a series of bound states forms with the majority of the probability distribution $|\Psi|^2$ above the surface (b).

and a binding energy

$$E_n = \frac{\mathrm{Ry}}{16}\frac{1}{(n+a)^2} \ , \tag{3.3}$$

which is reduced by a factor of 16 compared to the binding energy Ry = 13.6 eV of the hydrogen atom. The quantum defect a accounts for the finite penetration of the wave function into the metal. In other words, a describes the (complex) reflectivity of the crystal, which depends on the position of the image-potential state in the gap of the surface-projected bulk bands. In a Shockley-inverted gap, where the gap is p-like at the bottom and s-like at the top, the value of a ranges from 0.5 at the bottom of the band gap to 0.0 at the top of the band gap [162].
The maximum of the probability density of the image-potential-state electrons lies a few Ångstrom above the surface, the distance increasing quadratically with the quantum number n. Parallel to the surface the electrons can move freely, undisturbed by the surface corrugation, with an effective mass close to the free-electron value [125].

3.2 ... on ferromagnetic surfaces

In a ferromagnet, the electronic bands are exchange-split, and it was expected that the interaction of the image-potential states with the surface of the ferromagnet lift the spin degeneracy of these states [27]. In a multiple scattering approach (originally developed by Echenique and Pendry [49]), the two subsystems of majority and minority spin can be treated separately, and the different positions of the spin up and spin down bulk band edges yield a spin-dependent crystal barrier. Hence a spin-dependent quantum defect is required to calculate the binding energy of the image-potential state in front of a ferromagnetic metal

$$E_n^{\uparrow\downarrow} = \frac{\mathrm{Ry}}{16}\frac{1}{(n+a^{\uparrow\downarrow})^2} \ . \tag{3.4}$$

Consequently, the spin splitting

$$\Delta E_n = E_n^{\uparrow} - E_n^{\downarrow} \approx \frac{\mathrm{Ry}}{16}\frac{a^{\downarrow} - a^{\uparrow}}{n^3} \tag{3.5}$$

is expected to scale with n^{-3} for large n.
Since the image-potential is induced by screening from the electrons near the Fermi level, where the ferromagnetic surface usually has a spin-dependent density of states [185], the image potential experienced by electrons outside

the metal is also spin dependent due to exchange interaction near the crystal surface [118]. In the case of Fe(110), Nekovee and coworkers showed that due to the negative polarisation of the charge density in the surface layer, the contribution of the image-potential barrier, though comparatively small, has a sign opposite to the crystal barrier potential.
It was indeed found with spin-resolved inverse photoemission that the first image-potential state on the Ni(111) and the Fe(110) surface possesses a magnetic exchange splitting [123, 124].

3.3 Spin-resolved two-photon photoemission

Image-potential states are usually unoccupied as they are pinned to the vacuum level and the work function $\Phi = E_{\mathrm{vac}} - E_F$ of most metals exceeds their binding energy of below one electronvolt by far. Besides inverse photoemission (i. e. the detection of photons emitted by an incoming electron upon relaxation into an empty state), which proved its prowess in the detection of (spin-split) image-potential states, and scanning tunnelling spectroscopy, a local probe, two-photon photoemission (2PPE) is a powerful technique to access excited states. It is the particular ability to study excited electrons not only in the energy but also in the time domain, which made 2PPE so very successful. Since image-potential states were detected for the first time with 2PPE [65], many review articles gave a wonderful overview of the phenomena observable with 2PPE [71, 132, 182, 122, 51, 56, 180, 48].
In 2PPE, a first laser pulse (with photon energy $\hbar\omega_a$) excites an electron from an occupied bulk or surface state below the Fermi level E_F into an unoccupied state and from there a second laser pulse ($\hbar\omega_b$) raises the excited electron above the vacuum level E_{vac}. This is shown schematically in Fig. 3.2. The photoelectrons are then selected by energy and, in our case, their spin polarisation is determined. In order to avoid direct photoemission, which would overwhelm the second-order signal of 2PPE, the photon energy of the pump photon $\hbar\omega_a$ is kept below the work function of the sample, while chosen high enough to excite the image-potential states just below the vacuum energy E_{vac}.
The panel on the right hand side of Fig. 3.2 shows a typical spectrum obtained in the energy-resolved mode of 2PPE. The kinetic energy is defined with respect to the sample. The low-energy cut-off stems from direct photoemission. Due to the spectral width of a femtosecond laser pulse it can prove difficult to excite the higher order image-potential states without observing direct photoemission. The resonances (or peaks) associated with the first

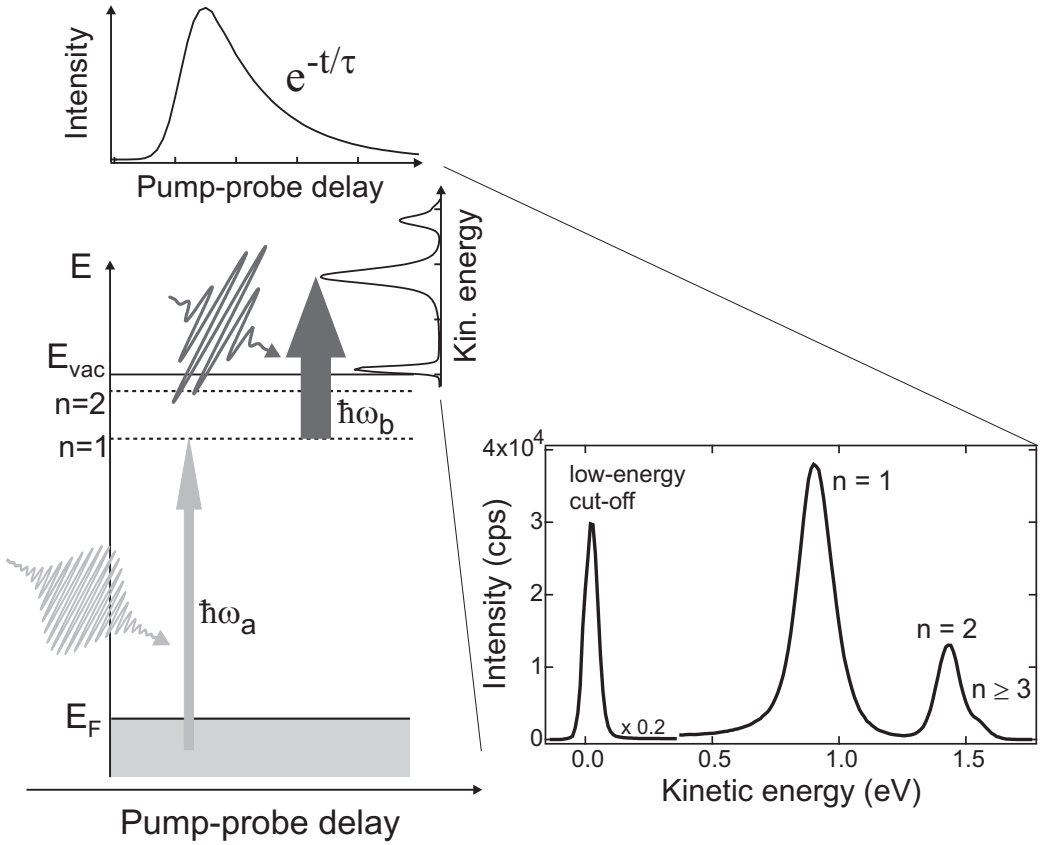

Figure 3.2: Schematic of two-photon photoemission; Right: Energy-resolved spectrum obtained after excitation by two photons of energies $\hbar\omega_a$ and $\hbar\omega_b$; The kinetic energy is defined with respect to the sample. Top: Intensity as a function of delay between pump and probe photon at fixed kinetic energy.

and second image-potential state are clearly discernible, while the states with $n \geq 3$ only show up as a shoulder on the high-energy tail of the $n = 2$ resonance. The excitation from bulk states into image-potential states scales with the penetration of the wave function into the crystal, i.e. with the overlap between the image-potential state and the initial bulk state [131, 91]. Photoemission from the image-potential states into the vacuum is also stronger for the image-potential states closer to the surface, because the gradient of the unperturbed image-potential $\nabla_z V(z)$ enters into the excitation probability [138] (these arguments will be discussed in more detail in the following sections; also cf. Equation 3.4). Hence the intensity of the image-potential resonances decreases with increasing quantum number n.

In the time-resolved mode of 2PPE (upper panel of Fig. 3.2) the energy of the electron analyser is held constant at the peak maximum of the respective state of interest while the intensity is recorded as a function of pump-probe delay. Thus the exponential decay of the population in the state can be monitored directly. Measurements of the time-resolved kind and their implications will be discussed extensively in Chapter 4.

The upper panel of Figure 3.3 shows a spin-resolved two-photon-photoemission spectrum of a 3 monolayer iron film on Cu(100). The majority component indicated by a black triangle clearly stands out against the minority component (open inverted triangles). The exchange splitting of the first $\Delta E_1 = 56 \pm 5$ meV and of the second image-potential state $\Delta E_2 = 7 \pm 3$ meV scales with the penetration depth of the image-potential state into the crystal, i.e. with n^{-3} as was discussed in Section 3.2. The exchange splitting of the image-potential states on a 6 monolayer cobalt film on Cu(001) (cf. lower panel of Fig. 3.3) with $\Delta E_1 = 27 \pm 5$ meV and $\Delta E_2 = 6 \pm 3$ meV is considerably smaller than on iron.

Since the exchange splitting mirrors the spin-dependent (and material dependent) bulk-band-gap boundaries (and the energetic position within the gap), a material dependence of the spin spitting is not unexpected. The smaller exchange splitting observed on the cobalt films may be due to the position of the image-potential state nearer the middle in the surface-projected band gap. On Fe the upper edge $X_{4'}$ of the *sp* band at the X point, which constitutes the lower edge of the crystal barrier for the image-potential states, lies approximately 500 meV higher above E_F than on Co [105]. Closer to the edges the image-potential-state wavefunction penetrates further into the bulk, increasing the influence of the exchange-split bulk bands [43].

A closer look at the spin-resolved spectra reveals several intriguing details. It is for example obvious that the relative intensity of the minority component

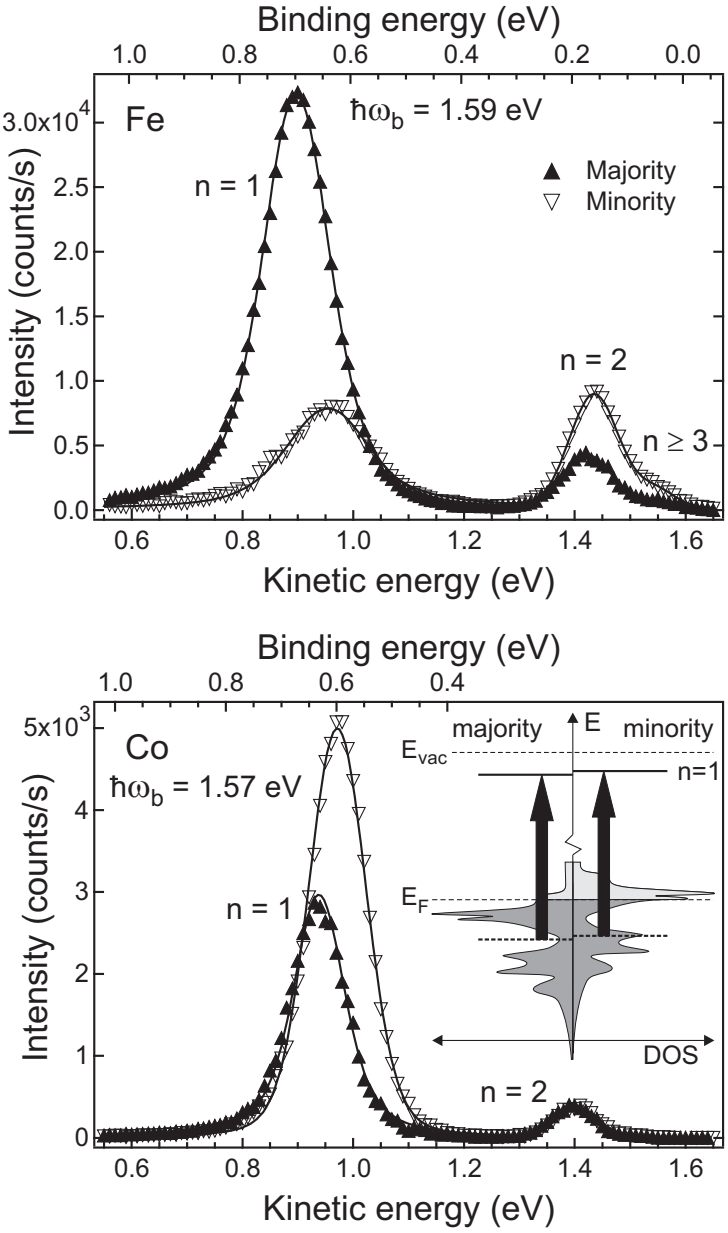

Figure 3.3: Spin- and energy-resolved 2PPE spectra of 3 ML Fe/Cu(100) (top) and 6 ML Co/Cu(100) (bottom). The exchange splitting between majority (▲) and minority (▽) components on Co is slightly smaller than on the Fe film. Note that throughout this work experimental uncertainties are within the symbol size where no error bars are displayed.

in the first and second image-potential state on iron does not obey an n^{-3} law. The reader may also note the spin-dependent intensities in the image-potential-state resonances. The spin polarisation is clearly strongly energy and material dependent[1].
This is not entirely surprising because the image-potential states are excited from the strongly exchange-split bulk states. One would consequently expect a spin-dependent density of states at the initial-state energy, $\hbar\omega_a$ below the image-potential-state energy (indicated schematically in the inset in Fig. 3.3). In the photo-excitation process the spin is conserved and the spin-dependent density of states is "projected" onto the image-potential states. As the second image-potential state lies roughly 500 meV above the first, their spin polarisation may of course also differ.
Unfortunately the strength of an optical excitation is not only determined by the density of states at the corresponding energy, but governed by dipole selection rules on the basis of symmetry considerations. We will therefore have a closer look at light-induced transitions in the next section.

3.4 Excitation into image-potential states

In a non-relativistic single-particle picture, the Hamiltonian of an electron interacting with the vector potential $\mathbf{A}(\mathbf{r},t)$ of an electromagnetic wave can be written as [157]

$$H_{\text{int}} = \frac{1}{2m}\left[-\frac{2e\hbar}{ic}\mathbf{A}\cdot\nabla - \frac{e\hbar}{ic}(\nabla\cdot\mathbf{A}) + \frac{e^2}{c^2}|\mathbf{A}|^2\right] . \tag{3.6}$$

The last term is small and can be neglected for the field strengths encountered with our laser. Due to the presence of the surface potential, the term $(\nabla\cdot\mathbf{A})$ can not be suppressed by choice of gauge. It is the source of surface emission and can considerably alter the lineshape of photoemission peaks from bulk states, but does not contribute to photoemission from surface states [108, 48, 70]. In the electric dipole approximation we can also substitute $\mathbf{A}(\mathbf{r},t)$ with $\mathbf{A}(t)$. Then, the optically driven transition rate between an initial state $|i\rangle$ and a final state $|f\rangle$ is described by Fermi's golden rule as

$$w_{fi} \propto |M_{fi}|^2\delta(E_f - E_i - \hbar\omega)\cdot\delta(\mathbf{k}_\parallel^f - \mathbf{k}_\parallel^i - \mathbf{g}_\parallel) , \tag{3.7}$$

[1]Of course, and this will become clear once the time-resolved measurements are discussed, the intensity of an image-potential-state peak in 2PPE depends strongly on the pump-probe delay and, for a fixed pump-probe delay, the intensity depends on the lifetime of the excited state. This must be taken into account in an interpretation of the energy-resolved spectra in terms of excitation strengths from the various initial state bands.

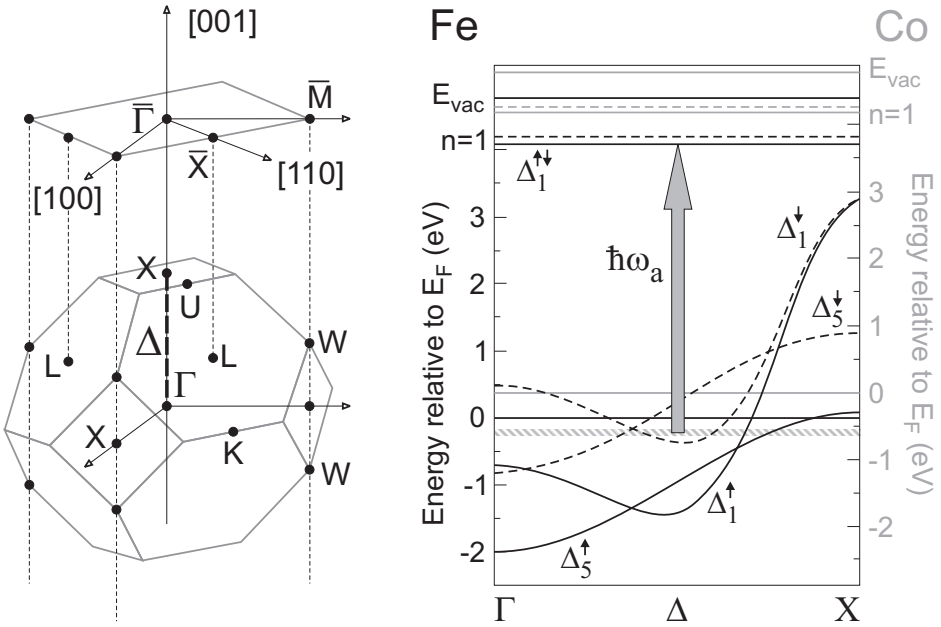

Figure 3.4: Bulk and surface Brillouin zone of an fcc(100) surface with high symmetry points (left). Dipole transitions into a surface state at $\bar{\Gamma}$ take place from states along Δ. Non-relativistic band structure of Fe/Cu(100) (left energy scale) and Co/Cu(100) (right energy scale) for the dipole-allowed initial states along Δ (right). Majority- (minority-) spin states are indicated with solid (dashed) lines.

where the matrix element M_{fi} is proportional to the remaining interaction operator

$$|M_{fi}|^2 \propto |\mathbf{A}\cdot\langle f|\mathbf{p}|i\rangle|^2 \propto |\mathbf{A}\cdot\langle f|\mathbf{r}|i\rangle|^2 \propto |\mathbf{A}\cdot\langle f|\nabla V|i\rangle|^2 \,. \qquad (3.8)$$

The two terms on the right are alternative (and sometimes more convenient) representations of the interaction operator, derived with the help of the commutation relations of $\mathbf{p}$ and $\mathbf{r}$ with the unperturbed Hamiltonian [179]. In the electric dipole transition energy and momentum are conserved, as is indicated by the δ-functions. Image-potential states, however, are localised at the surface, where the translational symmetry is broken and thus for excitation into a surface state only the wave vector parallel to the surface $\mathbf{k}_\parallel$ is conserved (modulo surface reciprocal lattice vectors $\mathbf{g}_\parallel$) [85, 138].

We can now evaluate the excitation probability w_{fi} on the basis of symmetry considerations and dipole selection rules. This will allow us a qualitative interpretation of our spin-resolved 2PPE spectra.

The left panel of Fig. 3.4 shows the bulk and surface Brillouin zone of an fcc(100) surface (after [138, 180]). Excitation into the image-potential state

at the $\bar{\Gamma}$-point of the surface Brillouin zone takes place from bulk states along the Δ direction ($\Delta = \Gamma - X$; highlighted by the thick dashed line). Due to dipole selection rules [47], in our experimental setup only states with Δ_1 or Δ_5 symmetry are allowed as initial states in the excitation with *p*-polarised light. Excitation with *s*-polarised light is possible from Δ_5 states only. Hence, in the (non-relativistic) band structure[2] of the magnetic pseudomorphs Fe/Cu(100) and Co/Cu(100) along the Δ direction (after [105]; a relativistic band structure for fcc Co may be found in [153]), only the majority-spin and minority-spin bulk states of Δ_1 and Δ_5 symmetry are shown (cf. Fig. 3.4, right hand side). The image-potential states are of Δ_1 symmetry. They are localised at the surface and consequently display no dispersion perpendicular to the surface.
Now, possible initial states for an excitation with a photon of energy $\hbar\omega_a$ can be found at every wave vector along Δ, $\hbar\omega_a$ below the image-potential state energy. Here one has to keep in mind that the spectral width of the pump pulse introduces a certain uncertainty in energy, just like the probe pulse width enters into the energy resolution for the image-potential states. Provided the image-potential state is primarily derived from a single bulk band, the portion of the image-potential-state wavefunction inside the metal has the same periodicity as the bulk states at the Brillouin zone boundary X. Therefore the transition matrix element M_{fi} is largest for initial states near the X point, decreasing towards Γ [104]. In addition, as the image-potential states reside in the *sp* band gap, they are of similar character as the *sp* bulk states. This leads to a weaker excitation from *d* bands (of Δ_5 symmetry) compared to excitation from *sp* bands (of Δ_1 symmetry) [177], a fact which is quite obviously supported by experiment: The intensities obtained with *s*-polarised light, where excitation occurs from Δ_5 bands only, are considerably smaller than the intensities encountered with *p*-polarised light (cf. next section). From a density of states argument alone, one would have probably drawn a different conclusion here, because the flat dispersion of the *d* bands suggests a high density of states.

3.5 Sampling the band structure

With the considerations described in the previous section, and keeping in mind that the spin of the electron is conserved in the excitation process, the

[2]For the moment we will consider a non-relativistic band structure and postpone the discussion about spin-orbit coupling and dichroism in photoemission until Section 3.6.

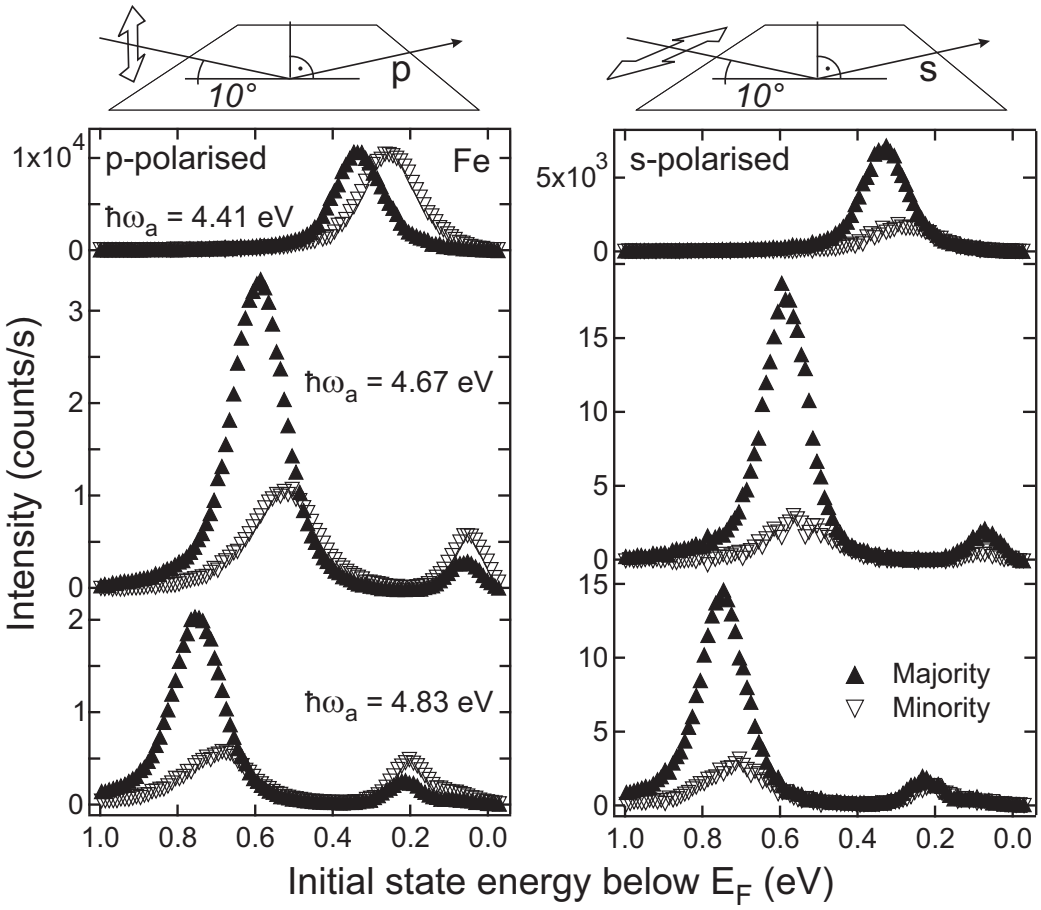

Figure 3.5: Spin- and energy-resolved 2PPE spectra of 3 ML Fe/Cu(100), taken with p-polarised (left) and s-polarised (right) pump light. Plotting the spectra on an initial-state energy-scale shows that upon changing the energy of the pump pulse, the image-potential state is excited from different initial bulk states (Δ_5 states for s light and Δ_5 or Δ_1 states for p light).

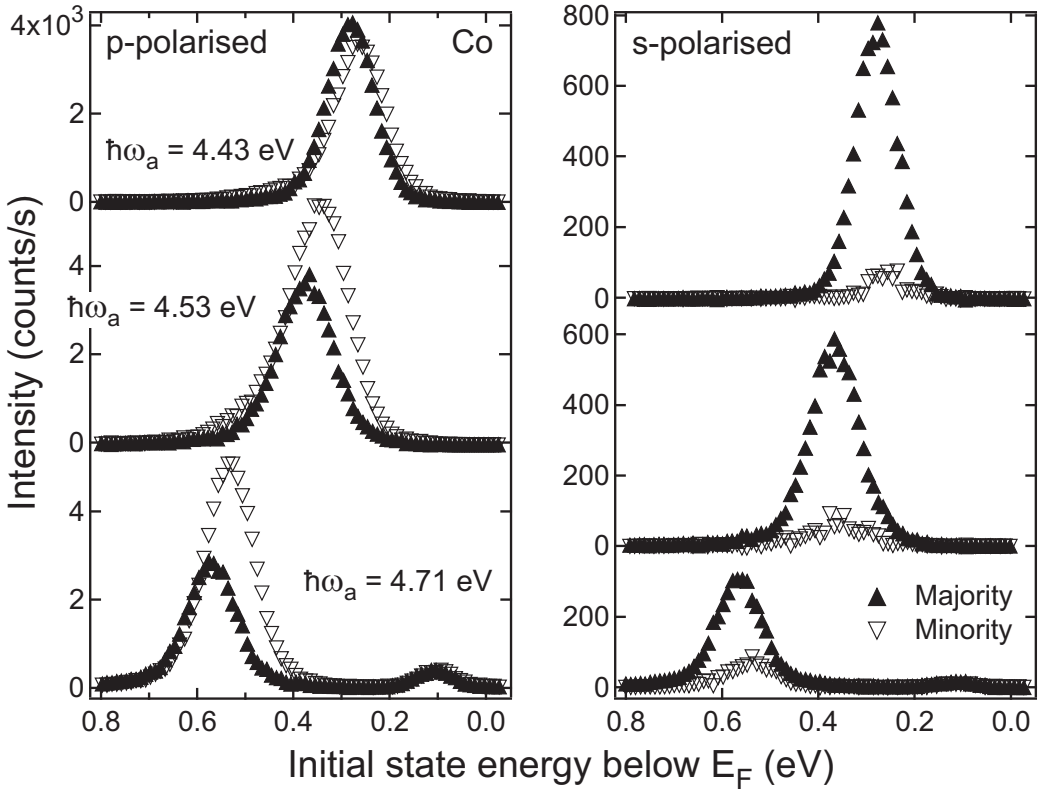

Figure 3.6: Spin- and energy-resolved 2PPE spectra of 6 ML Co/Cu(100), taken with *p*-polarised (left) and *s*-polarised (right) pump light and plotted on an initial-state energy-scale. The strong minority component in the left hand spectra stems from the surface state 0.4 eV below the Fermi energy.

observed spin-dependent intensities in the $n = 1$ and $n = 2$ image-potential states on Fe and Co films can be explained qualitatively.
The spectra taken with s-polarised pump light (right panel in Figs. 3.5 and 3.6, respectively) are dominated by majority-spin electrons. The $\Delta_5^\downarrow$ band crosses the Fermi level already close to the Γ point, leaving only the $\Delta_5^\uparrow$ band filled near the X point, where the excitation is strong.
The weak minority contribution to the $n = 1$ state on Fe, when pumping with p-polarised light, might be due to the position of the $\Delta_1^\downarrow$ band. To occupy the $n = 1$ state from this band with a photon energy of $\hbar\omega_a$, the lowest point may not be more than $\hbar\omega_a - E(n = 1)$ below E_F ($E(n = 1)$ relative to E_F). It seems that the band bottom is too high to occupy the $n = 1$ state, but perfect as initial state for the population of the higher image-potential states, which are strongly negatively spin polarised.
It becomes clear that spin-resolved 2PPE measurements are highly sensitive to the spin-split band structure. With a variation of the energy and polarisation of the pump pulse, these measurements may contribute to a confirmation and refinement of previous band structure models for thin magnetic films.
So far this was done systematically for 3 monolayers Fe on Cu(100) and 6 monolayers Co an Cu(100) by my colleague M. Pickel [135]. In a careful analysis of the spin polarisation as a function of initial state energy, he could confirm the band structure shown in Fig. 3.4 in principle, while adding values for the extremal points of the bands and increasing their accuracy. He concluded that the Co film is a strong ferromagnet with the majority d band fully occupied. The band maximum at X lies 0.2 eV below the Fermi energy, the band maximum marked by a sharp drop in the spin polarisation of the photoemission peaks. Fe, on the other hand, shows no such behaviour, indicating that the thin pseudomorphic fcc film is a weak ferromagnet with unoccupied majority d states above E_F, much like its bulk bcc counterpart. In addition, on the Co film a surface state 0.45 eV below E_F was found. This state is of minority-spin character and serves as initial state in the population of the (minority) image-potential state with a high probability due to the large spatial overlap of the surface states. The surface state is visible in the spectra measured with p-polarised pump light as a strong minority feature in a narrow initial-state-energy window [135]. The existence of a minority-spin surface state was also confirmed with high resolution spin- and angle-resolved photoelectron spectroscopy [111], but the surface state is quenched upon adsorption of cesium [4].
The determination of the band structure as described above is of a qualitative manner rather than quantitative, as long as our measurements can not be

compared with a (relativistic) band structure explicitly calculated for the thin films.
Moreover, some points of the argumentation so far might not be strictly valid in our case. The field vector of our p-polarised light has a major component along z, perpendicular to the surface, as the angle of incidence is 80°. It is therefore tempting to assume that excitation can occur from sp states only, because we have mainly Δ_1 light. Inside the metal however, the electromagnetic vector potential has to be calculated from the incident light $\mathbf{A}_{\text{in}}$ with macroscopic Fresnel equations[3], taking into account the dielectric constant[4] [108]. This can have a strong influence on the relative amplitude of the two field components parallel and perpendicular to the surface, increasing the probability for excitation from d states [30]. Only due to the overall low excitation strength from d states, might it be nevertheless safe to assume that excitation occurs mainly from sp states.
Due to the presence of the magnetic d states, the qualitative arguments for the excitation process discussed up to here might not be strictly applicable, as they were mostly developed for noble metal surfaces. We know from Section 3.2 that the d states participate strongly in the screening of the image-potential-state electrons, definitely influencing the image potential and possibly the wave function inside the metal. Also iron, for example, shows a strong hybridisation of sp with d states [170], a fact which might very well influence the relative excitation cross sections between sp and d states.

3.6 Dichroism

Up to now, we have based our discussion on a non-relativistic band structure, where spin-orbit coupling is neglected, the very effect which allows us to measure with spin resolution.
A very nice and thorough overview of the effects of spin-orbit coupling on the band structure and consequently on photoemission, with the experimentalist's need in mind, can be found in [100]. I will only give a very short introduction here, mainly based on this review article.
Spin-orbit coupling connects the spin to the three-dimensional space, cou-

[3]Note that in this approach $\nabla \cdot \mathbf{A} = 0$ is assumed.

[4]While the dielectric constant is well known for most bulk metals, it is not clear how the dielectric constant changes from its vacuum value to its bulk value at the surface, where the excitation into image-potential states occurs. A recent study suggests that the application of Fresnels equations with bulk optical constants is justified even for photoemission from surface states, provided the special geometry of focused light is taken into account [70].

pling spin and orbital parts of the electronic wave functions. The wave function is then written as a two-dimensional spinor

$$\Psi = \phi_a(\mathbf{r})|\uparrow\rangle + \phi_b(\mathbf{r})|\downarrow\rangle \ , \tag{3.9}$$

containing a linear combination of the two spin characters $|\uparrow\rangle$ and $|\downarrow\rangle$ [157, 100].

The selection rules introduced in Section 3.4 can be extended to account for spin-orbit coupling. As in the non-relativistic case, the dipole operator acts only on the spatial part of the wave function, for which the dipole selection rules remain valid, while the spin is conserved in the excitation process. Because the spin components $|\uparrow\rangle$ and $|\downarrow\rangle$ of Ψ are coupled to wave functions $\phi_{a,b}(\mathbf{r})$ of different spatial character, in general a photoelectron emitted from a (non-magnetic) material with sufficiently high spin-orbit coupling is spin polarised [181]. This process is called optical spin orientation[5].

If the initial state is already spin polarised, as is the case in a ferromagnet, the optical spin-orientation influences the *intensity* of the photoexcited electrons as well, an effect referred to as magnetic dichroism. This means that in the presence of spin-orbit coupling we may encounter different spectra for two different experimental geometries if they are inequivalent with respect to the symmetry point group of the sample. The photon and electron momentum, $\mathbf{q}$ and $\mathbf{k}$, the polarisation of the light $\mathbf{A}$ and the direction of the magnetisation $\mathbf{M}$ enter into the characterisation of an experimental geometry.

In the Co samples, the in-plane magnetisation lowers the rotational symmetry from the fourfold $C_{4\mathrm{v}}$ point group of the crystal surface to a twofold point group $C_{2\mathrm{v}}$. The 3 ML iron films are not affected, because of their out-of-plane easy axis. In our experimental configuration, the two magnetisation directions of the in-plane magnetised Co sample are not equivalent, if we excite with p-polarised light. The 2PPE spectra in Fig. 3.7 show the different intensities $I(\downarrow)$ and $I(\uparrow)$ for the two antiparallel directions of magnetisation. To underline the effect, the asymmetry defined as $I(\downarrow) - I(\uparrow)/I(\downarrow) + I(\uparrow)$ is plotted on the right axis. Note that the $n = 1$ and the $n = 2$ image-potential state show opposite behaviour upon reversal of magnetisation.

As discussed above, we expect also different intensities in each spin channel for different magnetisation directions. A spin-resolved spectrum of the Co

[5]Optical spin orientation is exploited in the generation of spin-polarised electrons. In GaAs for example, electrons with a high degree of spin polarisation can be excited into the conduction band with circularly polarised light [40]. The spin-polarised electrons emitted from the surface may be employed in inverse photoemission or electron energy loss experiments.

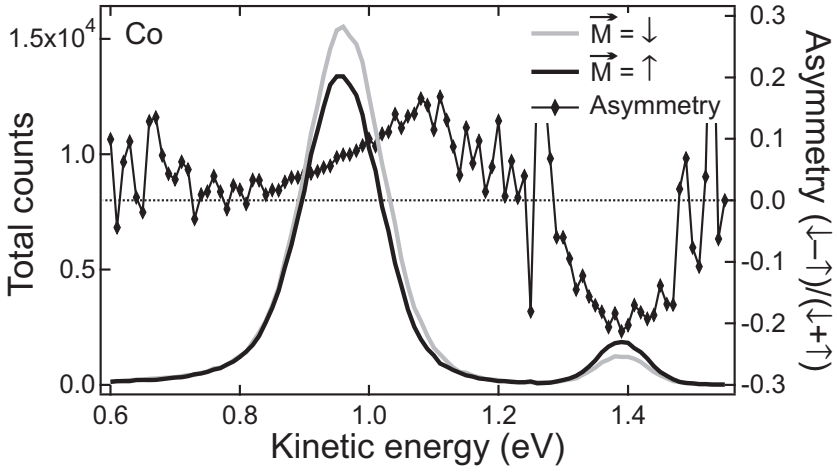

Figure 3.7: Energy-resolved (but spin-integrated) 2PPE spectra of the Co film for antiparallel directions of the magnetisation $\vec{M}$ measured with an excitation energy of $\hbar\omega_a = 4.78$ eV. The asymmetry $I(\downarrow) - I(\uparrow)/I(\downarrow) + I(\uparrow)$ of the intensity is plotted on the right axis.

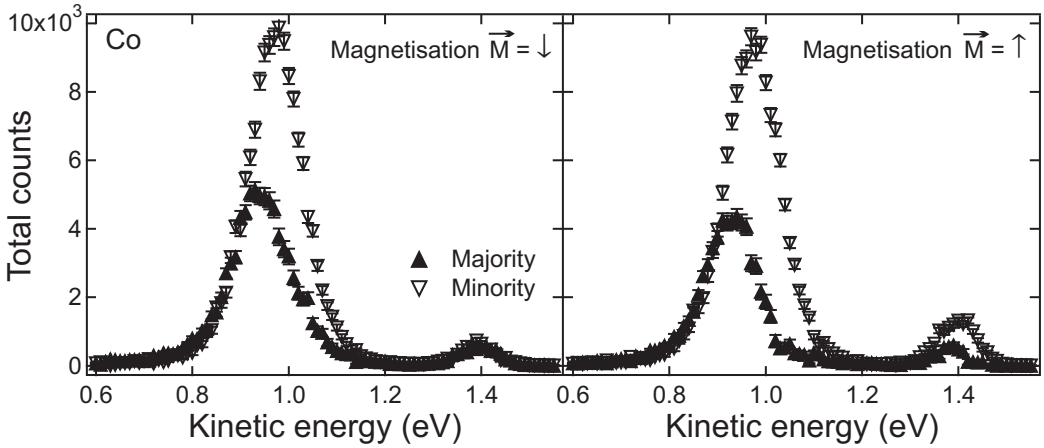

Figure 3.8: Due to spin-orbit split initial states, the spin polarisation and the intensity in the image-potential states may vary upon reversal of the magnetisation direction. For an excitation energy of $\hbar\omega_a = 4.78$ eV this is particularly pronounced in the $n = 2$ image-potential state.

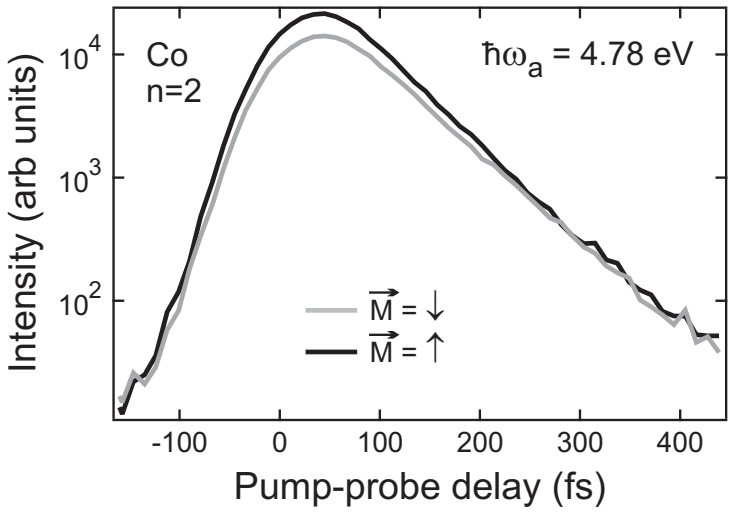

Figure 3.9: The time-resolved spectrum of the second image-potential state shows that we indeed observe magnetic dichroism. The spin-dependent lifetimes of the image-potential-state electrons in combination with the spin polarisation lead to different spin-averaged lifetimes for the two magnetisation directions.

sample (cf. Fig. 3.8) reveals that in the $n = 1$ image-potential state the majority-spin intensity changes slightly, while the minority component is strongly affected in the $n = 2$ image-potential state.
The next chapter will deal intensely with spin-dependent lifetimes, so I only shortly mention in advance that majority-spin electrons live longer than minority-spin electrons. Consequently we expect a state with more minority- than majority-spin electrons to decay faster on average. This is indeed the case for image-potential states on cobalt, where we observe lifetimes with (spin-integrated) 2PPE, which seem to depend on the direction of magnetisation (cf. Fig. 3.9). Of course this is exclusively by virtue of the dichroic nature of the excitation.

Effects of spin-orbit coupling

Spin-orbit coupling lowers the symmetry of a quantum mechanical system, thereby lifting degeneracies of electronic states. As a consequence, the symmetry character of the electronic states can no longer be described in terms of single group representations accounting for spatial symmetries only, but has to incorporate the spin space. Now hybridisation gaps occur at intersections between bands of the same double group character, but different (spatial) single group symmetry [80, 153, 100].

As magnetic dichroism is a reliable sign for the existence of spin-orbit split regions in the band structure, photoemission can be employed to find such cases. My colleague employed this technique to identify at least one such point in the band structure of thin cobalt films and determined its double group symmetry character [135].
Most intriguingly, spin-orbit coupling can lead to a mixture of majority- and minority-spin bands, where two bands with the same double group character but different spin character cross. Near such points, spin alone is no longer a good quantum number and in particular not necessarily conserved in a scattering event. This Elliott-Yafet spin-relaxation mechanism, i.e. the possibility that scattering includes a spin-flip transition, is a direct consequence of the mixing of electron states with opposite spin [52, 186].
While in semiconductors other spin-relaxation mechanisms play an equally important role, it is generally believed that the Elliott-Yafet mechanism by far dominates spin relaxation in metals [197]. The spin-relaxation time in metals, however, is not determined by the average strength of spin-orbit coupling, but rather by anomalies (e.g. due to spin-orbit coupling) at critical points in the band-structure. Here scattering processes may exhibit an Elliott-Yafet-type spin-flip probability several orders of magnitude larger than estimated from spin-orbit induced intermixing of majority- and minority-spin bands. Such "spin hot spots" in the band structure have a dominant influence on the spin dynamics in metals [53].
As mentioned in the introduction, Koopmans and coworkers suggested that in the presence of "spin hot spots" the Elliott-Yafet spin-flip probability for electron-phonon scattering might suffice to explain laser-induced demagnetisation on a timescale far below the electron-lattice relaxation time [95]. With the experimental access via dichroic features to potential "hot spots" in the band structure, we might be one step closer to unravel the mystery of ultrafast demagnetisation.